Hindawi
Mathematical Problems in Engineering
Volume 2020, Article ID 9701860, 16 pages
https://doi.org/10.1155/2020/9701860

Research Article

Impact of Temperature-Dependent Heat Source/Sink and Variable Species Diffusivity on Radiative Reiner–Philippoff Fluid

T. Sajid, M. Sagheer, and S. Hussain

Department of Mathematics, Capital University of Science and Technology, Islamabad, Pakistan

Correspondence should be addressed to T. Sajid; tanveer.sajid15@yahoo.com

Received 13 October 2019; Revised 28 December 2019; Accepted 28 February 2020; Published 22 April 2020

Academic Editor: Mariano Torrisi

The principle aim of the current communication is to scrutinize the impact of distinguished effects like variable thermal conductivity and variable molecular diffusivity on non-Newtonian Reiner–Philippoff fluid moving over a stretchable surface. The process of heat transfer is carried out in the presence of nonlinear thermal radiation, variable thermal conductivity, and heat generation/absorption. Furthermore, the study of mass transfer phenomena is carried out in the existence of variable molecular diffusivity. The PDEs regarding our model are renovated into ODEs by utilizing similarity transformation. Furthermore, the dimensionless model is tackled with the help of the RK4 method in conjunction with the shooting technique. The effects of different physical parameters that emerged during the numerical simulation on mass transfer rate, heat transfer rate, and velocity field are portrayed in the form of tables and graphs. It is noteworthy that an elevation in the heat source/sink parameters causes a reduction in the temperature profile. Moreover, a positive variation in the species diffusivity parameter augments the mass fraction field. A variation in the fluid parameter is found to be significantly affecting the shear thinning and shear thickening behaviour of the fluid. Reliability of the numerical outcomes is judged by comparing the obtained outcomes with the already available literature. The article is unique in its sense that the heat and mass transfer analysis of Reiner–Philippoff fluid under the aforementioned effects has not been investigated yet.

1. Introduction

Non-Newtonian fluids have attracted the attention of scientists and engineers in the past years due to their enormous applications in the field of energy and technology. Daily life examples of non-Newtonian fluids are cosmetics, paper production, fiber technology, ketchup, toothpaste, paint, shampoo and blood, wall paint, greases, lubricants, plastic, drilling, mud, etc. All non-Newtonian fluids on the basis of their behaviour in shear are not predicted by a single relation. Several mathematical models have been developed to understand the behaviour of shear stress and strain phenomenon in non-Newtonian fluids. Among all, the Sisko model, Carreau viscosity model, Powell–Eyring model, viscoelastic model, Ellis model, cross viscosity model, and Reiner–Philippoff model are most important models to understand the nature of such fluids. The Reiner–Philippoff model belongs to a class of pseudoplastic/shear thinning fluid. A few number of research studies are available in the literature regarding the boundary layer nature of Reiner–Philippoff fluid. Kapur and Gupta [1] adopted the Karman–Pohlhausen method to find the numerical solution of 2D boundary layer flow of Reiner–Philippoff fluid passing through an inlet length of a straight channel. Ghoshal [2] pondered the impact of non-Newtonian Reiner–Philippoff fluid passing through a circular tube. Na [3] utilized the finite difference method to analyze the boundary layer flow of Reiner–Philippoff fluid over different body shapes like 90° stretching wedge and semi-infinite plate. Yam et al. [4] presented a numerical analysis of boundary layer flow of Reiner–Philippoff fluid flow across a 90° stretching wedge. Ahmed [5] examined the impact of nanoparticles on Reiner–Philippoff nanofluid past a stretching sheet. Ahmed et al. [6] adopted the nonlinear shooting method to find the numerical solution of Reiner–Philippoff fluid past a nonlinear stretching sheet with variable thickness. Reddy et al.

[7] successfully applied the shooting method to Reiner–Philippoff fluid flow across a stretching sheet accompanied with transverse applied magnetic field effect. Kumar et al. [8] examined the conduct of Cattaneo–Christov heat diffusion and magnetic field on Reiner–Philippoff fluid over a stretchable surface. Reddy et al. [9] studied the Darcy–Forchheimer flow of Reiner–Philippoff fluid past a linear stretching sheet accompanied with viscous dissipation and thermal radiation.

Radiation is actually the emission or transmission of energy in the form of waves or particles through space or any material medium. Objects emit radiation when electrons from high energy orbit falls down to lower energy orbits. The energy is emitted in the form of electromagnetic radiation. Radiation has immense applications in agriculture, space exploration, law enforcement, geology, glass generation, gas turbines, polymer preparation, spacecraft working at high temperature, furnace design, electricity generation, etc. The linear thermal radiation can be achieved by linearizing the Rosseland approximation [10] with the help of Taylor's series. Linearized Rosseland approximation has unique Prandtl number [11], whereas in the case of nonlinear Rosseland approximation, three key factors are involved in the problem, termed as Prandtl number, radiation parameter, and temperature ratio parameter. Nonlinear thermal radiation has various applications in industry like polymer production, nuclear reactors, and thermal furnaces. Rosseland approximation [11] for the radiative heat flux has been helpful in computing the heat transfer rate associated with an optically thick fluid. Pantokratoras scrutinized the impact of natural convection along a vertical isothermal plate with linear and nonlinear Rosseland approximation [10]. Linearized version of Rosseland approximation for thermal radiation is used where temperature difference is small. Kho et al. [12] studied the impact of thermal radiation on Williamson nanofluid past a stretching sheet with constant wall temperature. Hayat et al. [13] investigated two-dimensional stagnation point flow of Maxwell nanofluid past a permeable stretchable surface accompanied with thermal radiation. The impact of thermal radiation and chemical reaction on third grade fluid across an exponential stretching sheet was examined by Hayat et al. [14]. Waqas et al. [15] scrutinized the Jeffrey nanofluid flow over stretching sheet embedded with thermal radiation, stratification, and convective boundary conditions. Waqas et al. [16] modelled viscoelastic nanofluid including buoyancy forces, thermal radiation, and convective boundary conditions. Nonlinear thermal radiation is used for both small as well as high temperature difference. Some new literature regarding nonlinear thermal radiation may be found in Refs. [17–26].

The ability of material to conduct heat is called thermal conductivity. Thermal conductivity is a property of material that varies with temperature. There are two mechanisms behind thermal conductivity in fluids. First, when the collision of molecules increases, the exchange of energy increases which ultimately helps to transport heat energy through the medium. Second, the random movement of molecules increases in the presence of thermal conductivity. As random movement of molecules increases, it transports heat energy in a particular direction. It is observed that materials having high thermal conductivity are used in heat sink while materials with low thermal conductivity are used as thermal insulation. Thermal conductivity has important applications like electrolytes, steam generators, concrete heating, laminating, catalysis, and molding blow. Hayat et al. [27] scrutinized the conduct of variable thermal conductivity and Cattaneo–Christov heat flux on stratified Oldroyd-B fluid flow towards linearly stretched surface. Khan et al. [28] explored the impact of variable thermal conductivity and nonlinear thermal radiation on nanofluid flow across a moving thin needle. Reddy et al. [29] considered the Williamson nanofluid moving over a stretching surface along with MHD and variable thermal conductivity. Hayat et al. [30] treated the stratified Powell–Eyring fluid moving towards a nonlinear stretching surface along with variable thermal conductivity and Cattaneo–Christov heat flux. Kumar and Varma [31] studied the effect of variable thermal conductivity and variable molecular diffusivity on a nanofluid moving over a variable porous stretching sheet. Recently, some researchers have discussed variable thermal conductivity with different geometries [32–36].

Internal heat generation/absorption generates heat energy inside a body by the nuclear process or chemical reaction. There are two models available in literature to scrutinize the effect of heat source/sink on the body. In the first model, internal heat source/sink is uniformly temperature dependent, i.e., $Q_0 (T - T_\infty)$. The second model is temperature- and space-dependent heat source/sink model, also called nonuniform heat source/sink model mentioned in energy equation (5). Possible heat generation effects may change the temperature distribution and furthermore the particle deposition. In the present study, the effect of nonuniform heat source/sink has been debated in detail. Heat source/sink in moving fluids has various applications in industry like reactor safety analysis, spent nuclear fuel, combustion analysis, and metal waste. Hayat et al. [37] investigated the impact of heat generation and radiative radiation on fluid flow over a rotating disk along with velocity and thermal slip conditions. The impact of heat generation and magnetic dipole on ferromagnetic Williamson fluid flow over a stretchable surface was examined by Waqas [38]. Salem and Abd El-Aziz [39] scrutinized the effect of internal heat generation/absorption and Hall current on hydromagnetic flow over a stretching surface. Hayat et al. [40] pondered on the behaviour of internal heat generation/absorption, thermal radiation, and double stratification on Maxwell nanofluid fluid moving over a stretchable surface. The behaviour of a two-dimensional laminar boundary layer flow over a stretching surface accompanied with heat source/sink and linear thermal radiation was contemplated by Devi et al. [41]. Muthtamilselvan and Ramya analyzed the impact of heat source/sink on unsteady laminar flow of an incompressible electrically fluid flow towards a porous stretching sheet [42]. The impact of mixed convection, heat generation/absorption, and thermal stratification on an Oldroyd-B fluid past a stretchable surface was examined by Hayat et al. [43]. Few recent attempts in this direction may be represented by [44–50].

In the light of aforementioned literature, the purpose of current study is to analyze the behaviour of Reiner–Philippoff fluid past a stretching sheet accompanied with nonlinear thermal radiation, heat source/sink, variable thermal conductivity, and variable molecular diffusivity. The present research fills the gap not adequately addressed in existing literature with the points enumerated underneath.

(i) Heat and mass transfer analysis under the effects of variable thermal conductivity, nonlinear thermal radiation, nonuniform heat source/sink, and variable molecular diffusivity on Reiner–Philippoff has not been done yet.

(ii) Prior to this article, no comparison analysis in the case of Reiner–Philippoff has been available in the literature to check the reliability of numerical results obtained.

(iii) In the available literature, no work has been reported other than [5] to discuss the mass transfer analysis in the case of Reiner–Philippoff fluid.

(iv) The skin friction coefficient and especially local Sherwood number in the form of figures and tables on Reiner–Philippoff have not been deeply investigated in the available literature.

2. Mathematical Formulation

One of the traditional portrayals of the stress-deformation conduct of Reiner–Philippoff fluid [5–9] is

$$\frac{\partial u}{\partial y} = \frac{\tau}{\mu_\infty + \left((\mu_0 - \mu_\infty)/\left(1 + (\tau/\tau_s)^2\right)\right)}. \tag{1}$$

In the above equation, the expression in right side named as the flow function. The distinguished symbols such as τ, τ_s, μ_0, and μ_∞ indicate the shear stress, reference shear stress, zero shear viscosity, and limiting viscosity. Reiner–Philippoff fluid belongs to a class of non-Newtonian fluids which exhibits all three, dilatant, Newtonian, and pseudoplastic type, behaviours. The depicted flow function [5] is portrayed by

$$f(\sigma) = \frac{\sigma}{1 + ((\lambda - 1)/(1 + \sigma^2))}, \tag{2}$$

where $\sigma = \tau/\tau_s$ and $\lambda = \mu_0/\mu_\infty$. The behaviour of the fluid varies with change in λ. Fluid behaves like Newtonian in case of $\lambda = 1$, dilatant for $\lambda < 1$, and pseudoplastic for $\lambda > 1$.

Figure 1 reflects the geometrical conduct of two-dimensional non-Newtonian Reiner–Philippoff fluid moving over a stretched sheet with stretching velocity u_w acting along $x-$ axis. At the surface of the sheet, temperature and concentration are represented by T_0 and C_0. The symbols T_∞ and C_∞ indicate the ambient temperature and ambient concentration, respectively. The heat generation/absorption along thermal boundary layer is manifested by q'''. The effects like nonlinear thermal radiation and variable thermal are expected to affect the heat transfer process in the energy equation while the variable molecular diffusivity is assumed to affect the mass transfer phenomenon. Equations (3) and (4) depict the continuity and fluid flow phenomenon, whereas heat and mass transfer analysis in the present Reiner–Philippoff model is carried out by (5) and (6). The equations regarding continuity, momentum, energy, and concentration [5–9] are enumerated underneath:

$$\frac{\partial u}{\partial x} + \frac{\partial v}{\partial y} = 0, \tag{3}$$

$$u\frac{\partial u}{\partial x} + v\frac{\partial u}{\partial y} = \frac{1}{\rho_f}\frac{\partial \tau}{\partial y}, \tag{4}$$

$$\begin{aligned} u\frac{\partial T}{\partial x} + v\frac{\partial T}{\partial y} &= \frac{1}{\rho C_p}\frac{\partial}{\partial y}\left(\kappa\frac{\partial T}{\partial y}\right) + \frac{1}{\rho C_p}\frac{\kappa_\infty U_w(x)}{xv} \\ &\cdot \left[A^*(T_0 - T_\infty)e^{-\eta} + B^*(T - T_\infty)\right] - \frac{1}{\rho C_p}\frac{\partial q_r}{\partial y}, \end{aligned} \tag{5}$$

$$u\frac{\partial C}{\partial x} + v\frac{\partial C}{\partial y} = \frac{\partial}{\partial y}\left(D_B(C)\frac{\partial C}{\partial y}\right). \tag{6}$$

The boundary conditions associated with the above model are

$$\left.\begin{aligned} &y = 0 : u(x, y) = U(x), v = 0, T = T_w, C = C_w, \\ &y \longrightarrow \infty : u \longrightarrow 0, T \longrightarrow T_\infty, C \longrightarrow C_\infty. \end{aligned}\right\} \tag{7}$$

The variable thermal conductivity and variable molecular diffusivity [21] are given by

$$\begin{aligned} \kappa &= \kappa_\infty\left(1 + \epsilon_1\left(\frac{T - T_\infty}{T_0 - T_\infty}\right)\right), \\ D_B(C) &= D_{B_\infty}\left(1 + \epsilon_2\left(\frac{C - C_\infty}{C_0 - C_\infty}\right)\right). \end{aligned} \tag{8}$$

The Rosseland radiative heat flux [10, 11] used in (5) is premeditated by

$$q_r = -\frac{4\sigma^*}{3\kappa^*}\frac{\partial T^4}{\partial y} = -\frac{16\sigma^*}{3\kappa^*}T^3\frac{\partial T}{\partial y}, \tag{9}$$

where the symbols σ^* and κ^* stand for Stefan–Boltzmann constant and the mean absorption coefficient, respectively.

A similarity transformation [5, 6] under the effect of the stretching velocity $U(x) = U_0 x^{1/3}$ is given below:

$$\left.\begin{aligned} \psi &= \sqrt{U(x)xv}\, f(\eta), \\ \eta &= \sqrt{\frac{U(x)}{vx}}\, y, \\ \tau &= \rho\sqrt{U_0^3 v}\, g(\eta), \\ \phi(\eta) &= \frac{C - C_\infty}{C_0 - C_\infty}, \\ \theta(\eta) &= \frac{T - T_\infty}{T_0 - T_\infty}. \end{aligned}\right\} \tag{10}$$

Using the above variables, fd1(1) and (4)fd4–(6) have been transformed into the ODEs bestowed underneath:

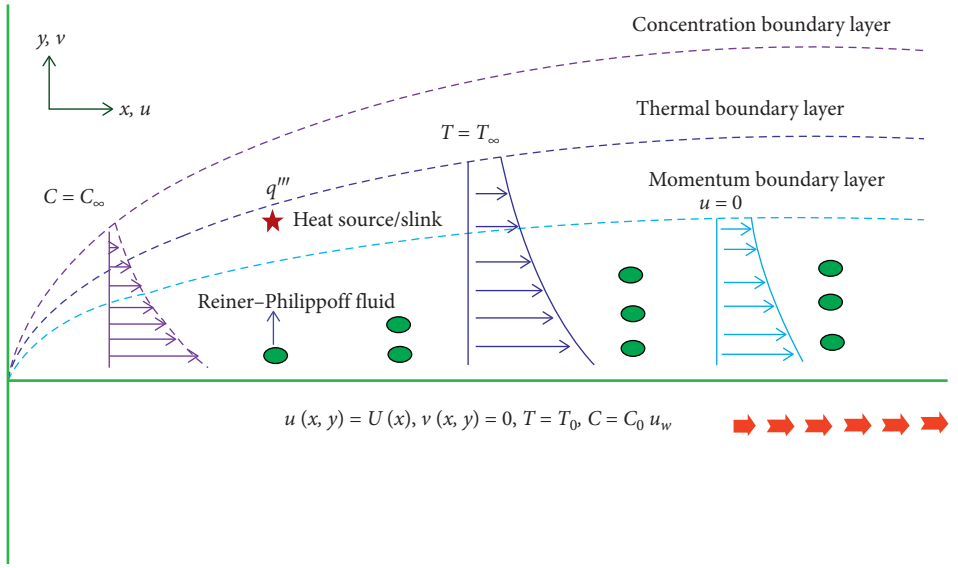

Figure 1: Physical configuration of the problem.

$$g' = \frac{1}{3}f'^2 - \frac{2}{3}ff'', \tag{11}$$

$$g = f''\frac{g^2 + \lambda\gamma^2}{g^2 + \gamma^2}, \tag{12}$$

$$\begin{aligned}&\left((1+\epsilon_1\theta) + \frac{4}{3}\mathrm{Rd}\left(1+(\theta_w-1)\theta\right)^3\right)\theta'' \\ &+ \left(\epsilon_1 + 4\mathrm{Rd}\left(\theta_w-1\right)\left(1+(\theta_w-1)\theta\right)^2\right)\theta'^2 \\ &+ \frac{2}{3}\mathrm{Pr}f\theta' + A^*e^{-\eta} + B^*\theta = 0,\end{aligned} \tag{13}$$

$$(1+\epsilon_2\phi)\phi'' + \frac{2}{3}\mathrm{Sc}f\phi' + \epsilon_2\phi'^2 = 0. \tag{14}$$

Furthermore, the boundary conditions in the dimensionless form are

$$\left.\begin{aligned}&\eta = 0 : f(\eta) = 0, f'(\eta) = 1, \theta(\eta) = 1, \phi = 1, \\ &\eta \longrightarrow \infty : f'(\eta) \longrightarrow 0, \theta(\eta) \longrightarrow 0, \phi(\eta) \longrightarrow 0.\end{aligned}\right\} \tag{15}$$

The distinguished parameters in (11)–(14) are given by

$$\left.\begin{aligned}\gamma &= \left(\frac{\tau_s}{\rho\sqrt{U_0^3\nu}}\right), \\ \lambda &= \frac{\mu_0}{\mu_\infty}, \\ \mathrm{Pr} &= \frac{\mu C_p}{k_\infty}, \\ \mathrm{Sc} &= \frac{\nu}{D_{B\infty}}, \\ Rd &= \frac{4\sigma T_\infty^3}{k^* k_\infty}, \theta_w = \frac{T_0}{T_\infty}.\end{aligned}\right\} \tag{16}$$

The surface drag coefficient is given by

$$Cf_x = \frac{\tau}{U_w^2/2}. \tag{17}$$

The dimensionless form of surface drag coefficient is given by

$$\frac{1}{2}Cf_x\mathrm{Re}_x^{1/2} = g(0). \tag{18}$$

The heat transfer rate is

$$Nu_x = \frac{xq_w}{k(T_0 - T_\infty)}, \tag{19}$$

where the term q_w indicates the heat flux which is manifested by

$$q_w = -k\left(\frac{\partial T}{\partial y}\right)_{y=0} + q_r. \tag{20}$$

The heat transfer rate in the dimensionless form is taken as

$$\mathrm{Nu}_x\mathrm{Re}_x^{-1/2} = -\left(1 + \frac{4}{3}\mathrm{Rd}\left((\theta_w-1)\theta(0)+1\right)^3\right)\theta'(0). \tag{21}$$

The local Sherwood number is given by the following formula:

$$\mathrm{Sh}_x = \frac{xq_m}{D_B(C_w - C_0)}. \tag{22}$$

The expression q_m represents the mass flux which is delineated by

$$q_m = -D_B\frac{\partial C}{\partial y}. \tag{23}$$

The dimensionless form of Sherwood number is

$$\mathrm{Sh}_x\mathrm{Re}_x^{-(1/2)} = -\phi'(0). \tag{24}$$

3. Solution Methodology

The above nonlinear system of equations (11)–(14) along with the boundary conditions (15) can be tackled by the utilization of the numerical technique termed as shooting method [51] for distinguished parameters arising during numerical simulation of the problem. Figure 2 is designed to describe the flowchart procedure of the shooting method.

For numerical solution, the unbounded domain $[0,\infty)$ has been replaced by $[0,\eta_{\max}]$ where $\eta_{\max}$ is a real number chosen in such a way that the solution does not show any significant variations for $\eta > \eta_{\max}$. It is noteworthy that $\eta_{\max} = 7$ assures the expected level of convergence for all the numerical outcomes delineated in this article. The momentum equations (11) and (12) will be tackled collectively by the shooting method and then the temperature and concentration equations will be tackled by using f as a known function. Denoting f by y_1, f' by y_2, g by y_3, and the missing initial condition by s, the momentum equations (11) and (12) are converted into the following system of first-order ODEs:

$$\left.\begin{aligned} y_1' &= y_2, && y_1(0) = 0,\\ y_2' &= \frac{y_3\left(y_3^2+\gamma^2\right)}{\left(y_3^2+\lambda\gamma^2\right)}, && y_2(0) = 1,\\ y_3' &= \frac{1}{3}y_2^2 - \frac{2}{3}y_1y_2', && y_3(0) = s. \end{aligned}\right\} \tag{25}$$

The above system (25) has been handled numerically with the assistance of the RK4. Furthermore, the missing initial conditions are updated with the help of Newton's scheme until the criteria stated below are met.

$$\max\left\{\left|y_2(\eta_{\max}) - 0\right|\right\} < \epsilon, \tag{26}$$

where the symbol ϵ is a positive number having value $\epsilon = 10^{-6}$ and $\eta_{\max} = 7$.

In order to solve the temperature equation (13), it is converted into the following system comprising of the first-order differential expressions (25) signifying θ by u_1 and θ' by u_2 and using f as a known function. The following system of ODEs together with the initial conditions is achieved.

$$\left.\begin{aligned} u_1' &= u_2, && u_1(0) = 1,\\ u_2' &= -\frac{\left[\left(\epsilon_1 + 4Rd\left(\theta_w-1\right)\left(1+\left(\theta_w-1\right)u_1\right)^2\right)u_2^2 + (2/3)\mathrm{Pr}fu_2 + \left(A^*\exp^{-\eta} + B^*u_1\right)\right]}{\left(\left(1+\epsilon_1u_1\right) + (4/3)\mathrm{Rd}\left(1+\left(\theta_w-1\right)u_1\right)^3\right)}, && u_2(0) = t. \end{aligned}\right\} \tag{27}$$

The system of equation (27) is treated the same way as (25) to obtain θ and θ'.

The concentration equation (14) is transformed into the first-order ODEs by denoting ϕ by z_1 and ϕ' by z_2 and taking f as a known function. The following resulting system of equations is achieved.

$$\left.\begin{aligned} z_1' &= z_2, z_1(0) = 1, z_2' = -\frac{\left(\epsilon_2 z_2^2 + (2/3)\mathrm{Sc}fz_2\right)}{1+\epsilon_2 z_1}, z_2(0) = u. \end{aligned}\right\} \tag{28}$$

Applying the same procedure on (28), the numerical solution of (14) can be obtained in the form of ϕ and ϕ'.

Table 1 presents the comparison analysis of current results with those reported by Reddy et al. [7] by fixing distinguished parameters $A^* = B^* = \epsilon_1\epsilon_2 = \mathrm{Sc} = 0$, $\mathrm{Rd} = 0.2$, $\theta_w = 0.9$, and $\gamma = 0.2$, whereas Table 2 depicts the comparison of local Nusselt number for present outcomes with Reddy et al. [9] by fixing $A^* = 0.1$, $B^* = 0.1$, $\epsilon_1 = 0.1$, $\epsilon_2 = \mathrm{Sc} = \theta_w = 0$, and $\mathrm{Pr} = 0.8$.

4. Results and Discussion

The current section revealed the impact of various parameters (raised during numerical simulation of the ODEs) on velocity, temperature, concentration profiles, skin friction coefficient, Nusselt number, and Sherwood number; moreover, such effects are portrayed in the form of tables. Table 3 reflects the influence of distinguished physical parameters that were raised during the numerical simulation of the model on the surface drag coefficient, heat transfer, and mass transfer. It is noted that a magnification in the Bingham number γ creates an augmentation in skin friction coefficient but situation is quite opposite in the case of the Reiner–Philippoff fluid parameter λ. In the case of heat transfer coefficient, a positive variation in the Reiner–Philippoff fluid parameter λ, thermal radiation Rd, temperature ratio parameter θ_w, and Prandtl number Pr produces an enlargement in the heat transfer rate but a reverse behaviour is monitored for the case of the remaining parameters such

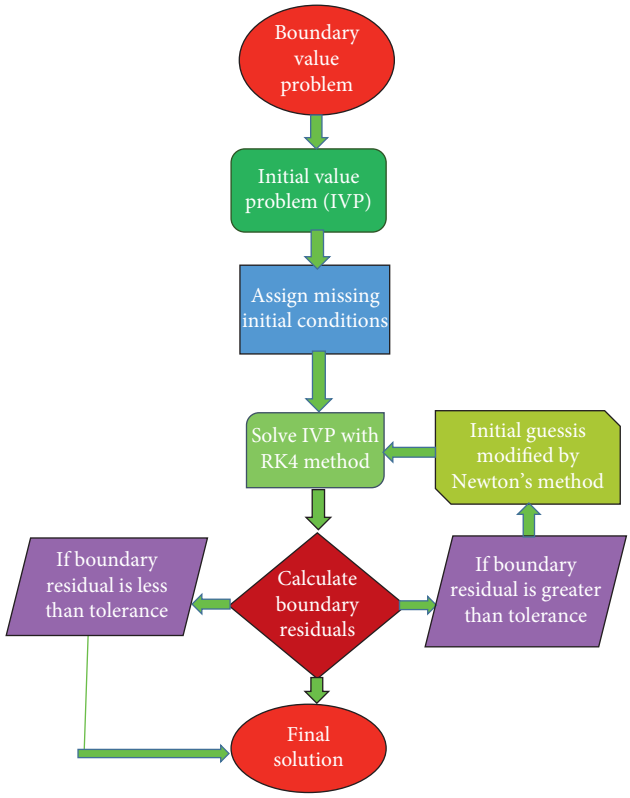

Figure 2: Mechanism of the shooting scheme.

Table 1: Comparison analysis of current results with those reported by Reddy et al. [7].

	$Nu_x Re_x^{-1/2}$	
	$\lambda = 1$	
Pr	Present	Reddy et al. [7]
1	0.556065	0.559879
1.5	0.727928	0.727497
2	0.873992	0.886106

Table 2: Comparison of local Nusselt number for present outcomes with Reddy et al. [9].

	Absence of Rd			
	$Nu_x Re_x^{-1/2}$			
	$\lambda = 0.5$		$\lambda = 1$	
γ	Present	Reddy et al. [9]	Present	Reddy et al. [9]
0.1	0.130909	0.109782	0.144535	0.114058
0.2	0.109284	0.102621	0.144535	0.114058
0.3	0.085161	0.097438	0.144535	0.114058

as the Bingham number γ, thermal conductivity ϵ_1, species diffusivity ϵ_2, heat generation/absorption coefficients A^* and B^*, and the Schmidt number Sc. The major factors responsible for an improvement in the mass transfer rate are λ and Sc. Furthermore, a conflicting effect on the mass transfer rate is being monitored in the case of γ and ϵ_2. Table 4 shows the fluctuation of distinguished parameters on the Nusselt number under the absence and presence of thermal radiation parameter by fixing Sc = 0.1 and $\epsilon_2 = 0.1$. From the table, it is quite clear that production of heat is more in nonlinear thermal radiation as compared to absence of thermal radiation.

Figure 3 highlights the impact of Bingham number γ on the velocity field. Bingham number γ is actually the ratio of the yield stress to the viscous stress. It is observed that the apparent viscosity increases by increasing shear rate. As a result, velocity profile depreciates. Figure 4 shows the impact of Reiner–Philippoff fluid parameter λ on the velocity profile. This parameter depicts the ratio of the zero shear viscosity to the upper Newton limiting viscosity. It is revealed from the figure that mounting the parameter λ guides to an abatement in the velocity field. It happens because the increasing values of λ cause a decrement in the viscosity which allows the fluid to move more freely. Figure 5 is portrayed to establish the impact of the Bingham number γ on the shear stress field. It is noted that an escalation in the parameter γ leads to an augmentation in the shear stress field. Physically, viscosity of the fluid decreases in the case of small Bingham number which consequently drives to an enhancement in the fluid shear stress. As a result, shear stress profile increases. As a result, shear stress field increases. The portrayal for nondimensional shear stress field against the Reiner–Philippoff fluid parameter λ is illustrated in Figure 6. It can be remarked that the shear stress field depreciates owing to an improvement in the parameter λ. It is quite clear that when the viscosity of fluid heightens, the shear stress rate of the fluid abates which guides to a reduction in the shear stress field. Figures 7 and 8 are plotted to illustrate the impact of heat generation/absorption parameters on the temperature field. It is revealed that enhancing the heat generation and absorption parameters A^* and B^*, more heat is generated inside the fluid which upsurges the thermal boundary layer thickness and ultimately guides to an augmentation in the temperature field. The variation of the temperature field versus the Prandtl number is plotted in Figure 9. Prandtl number is defined as the ratio of momentum diffusivity to thermal diffusivity. Physically, an improvement in the Prandtl number weakens thermal diffusivity which leads to an abatement in the thermal boundary layer thickness, which lessens the temperature within the boundary layer which causes a decrement in the temperature profile. Figure 10 is displayed to analyze conduct of temperature profile against the thermal conductivity parameter ϵ_1. It is found that when the collision of molecules increases, the exchange of energy increases which transports heat energy through the fluid and guides to an improvement in the variable thermal conductivity and temperature profile. Figure 11 is prepared for the analysis of the temperature field due to the diverse values of the thermal radiation parameter. Physically, nonlinear thermal radiation comprises of thermal radiation, temperature ratio parameter, and Prandtl number. Nonlinear thermal radiation is used where high temperature difference is required like glass, polymers, and nuclear reactors. It can be noted that an uplift in the radiation parameter delivers more heat to the fluid which leads to an embellishment in the fluid temperature. The impact of the temperature ratio parameter θ_w on the temperature field is portrayed in Figure 12. It is quite understood that by enhancing

Table 3: Variation in surface drag coefficient, heat transfer, and mass transfer rates.

γ	λ	Rd	θ_w	ϵ_1	ϵ_2	A^*	B^*	Pr	Sc	$(1/2)Cf_x\mathrm{Re}_x^{1/2}$	$\mathrm{Nu}_x\mathrm{Re}_x^{-1/2}$	$\mathrm{Sh}_x\mathrm{Re}_x^{-1/2}$
0.1	0.1	0.1	0.1	0.01	0.01	0.01	0.01	1.7	0.1	−0.660273	0.674889	0.133592
0.5										−0.380604	0.514999	0.118724
1										−0.246415	0.403716	0.113661
2										−1.143974	0.382161	0.112794
	0.3									−0.664497	0.673753	0.134262
	0.5									−0.668484	0.674594	0.134825
	0.7									−0.672282	0.675268	0.135308
		0.3								−0.660271	0.678065	0.133592
		0.5								−0.660271	0.683150	0.133592
		0.7								−0.660271	0.687991	0.133592
			0.3							−0.660271	0.674792	0.133592
			0.6							−0.660271	0.681787	0.133592
			0.9							−0.660271	0.694968	0.133592
				0.03						−0.660271	0.662843	0.133592
				0.05						−0.660271	0.653468	0.133592
				0.07						−0.660271	0.644409	0.133592
					0.03					−0.660271	0.672563	0.131896
					0.05					−0.660271	0.672561	0.130263
					0.07					−0.660271	0.672567	0.128701
						0.03				−0.660271	0.658104	0.133592
						0.05				−0.660271	0.643647	0.133592
						0.07				−0.660271	0.629192	0.133592
							0.03			−0.660271	0.656931	0.133592
							0.05			−0.660271	0.640894	0.133592
							0.07			−0.660271	0.624428	0.133592
								1.9		−0.660271	0.723241	0.133592
								2.1		−0.660271	0.771130	0.133592
								2.3		−0.660271	0.816659	0.133592
									0.3	−0.660271	0.672562	0.212701
									0.5	−0.660271	0.672562	0.296095
									0.7	−0.660271	0.672562	0.375564

Table 4: Impact of various parameters on Nusselt number in the presence and absence of nonlinear thermal radiation.

							$\mathrm{Nu}_x\mathrm{Re}_x^{-1/2}$					
							Absence of Rd			Presence of Rd		
γ	Pr	Rd	θ_w	A^*	B^*	ϵ_1	$\lambda = 0.5$	$\lambda = 1$	$\lambda = 1.5$	$\lambda = 0.5$	$\lambda = 1$	$\lambda = 1.5$
0.1	0.5	0.7	0.7	0.01	0.01	0.1	0.230013	0.233401	0.235598	0.303648	0.308120	0.311021
0.2							0.225131	0.233401	0.238479	0.297203	0.308121	0.314825
0.3							0.220087	0.233401	0.241094	0.290544	0.308120	0.318276
	1						0.377136	0.381290	0.383900	0.497870	0.503353	0.506800
	1.5						0.506331	0.509815	0.511972	0.668425	0.673024	0.675872
	2						0.618230	0.620843	0.622465	0.816146	0.819596	0.821738
		1					0.224120	0.22721	0.229223	0.326618	0.331120	0.334055
		1.5					0.217110	0.219789	0.221544	0.366048	0.370565	0.373524
		2					0.212224	0.214581	0.216131	0.406337	0.410851	0.413818
			1				0.174818	0.177595	0.179410	0.337984	0.343351	0.346859
			1.5				0.101348	0.102956	0.104032	0.420595	0.427268	0.431735
			2				0.065623	0.066399	0.066932	0.555611	0.562182	0.566693
				0.1			0.174185	0.177776	0.180104	0.229948	0.234689	0.237761
				0.2			0.112177	0.115995	0.118469	0.148089	0.153129	0.156395
				0.3			0.050191	0.054238	0.056859	0.066260	0.071602	0.075062
					0.02		0.211931	0.215703	0.218149	0.279776	0.284757	0.287986
					0.03		0.192580	0.196811	0.199551	0.254231	0.259816	0.263434
					0.04		0.171738	0.176520	0.179614	0.226718	0.233030	0.237114
						0.5	0.189140	0.192093	0.194015	0.24969	0.253588	0.256125
						1	0.157097	0.159651	0.161324	0.207389	0.210761	0.212969
						1.5	0.136128	0.138364	0.139839	0.179707	0.182660	0.184606

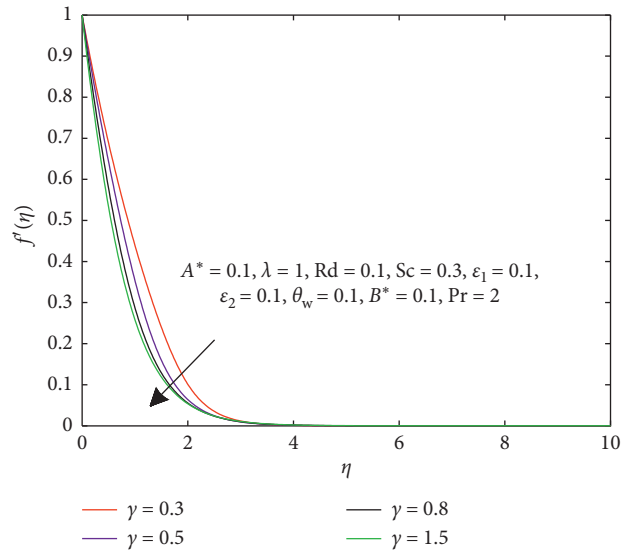

Figure 3: Influence of γ on f'.

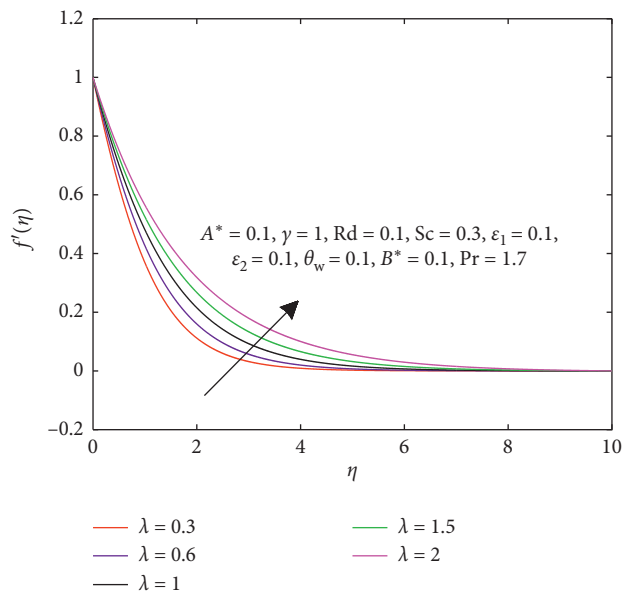

Figure 4: Influence of λ on f'.

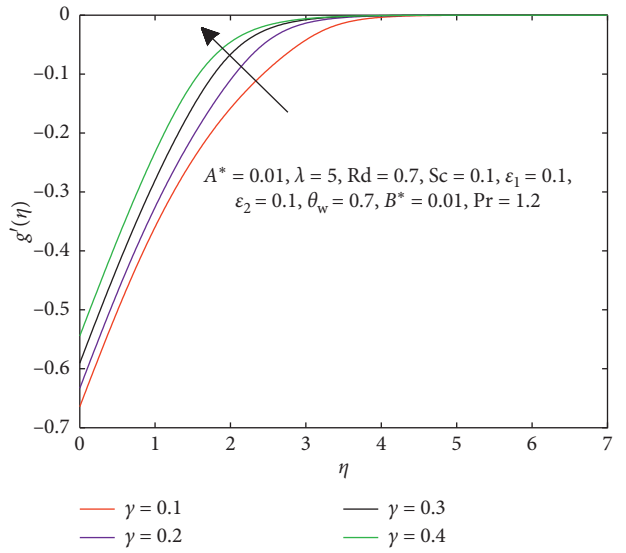

Figure 5: Influence of γ on g'.

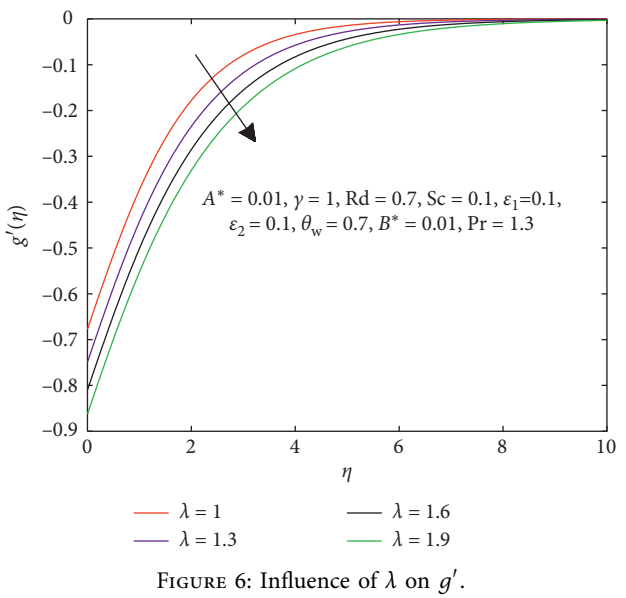

Figure 6: Influence of λ on g'.

temperature ratio parameter, more heat is generated which furthermore improves nonlinear thermal radiation and temperature field. Figure 13 is displayed to study the effect of the species diffusivity ϵ_2 on the mass fraction field. It is noticed that the growing value of ϵ_2 elevates the boundary layer thickness. It is quite clear that species diffusivity is proportional to concentration. A positive variation in the species diffusivity parameter heightens the mass fraction field. Figure 14 is plotted to observe the behaviour of the Schmidt number on the mass fraction field. Schmidt number is defined as the ratio of momentum diffusivity to molecular diffusivity. So, an augmentation in the Schmidt number causes a decrement in the concentration field because molecular diffusivity is inversely related to Sc. Figure 15 is sketched to demonstrate the conduct of Bingham number versus Reiner–Philippoff fluid parameter on the skin friction coefficient. Bingham number is defined as the ratio of yield stress to viscous stress. Physically, when Bingham number increases, the viscosity of fluid decreases (shear thinning) which ultimately guides to an abatement in the Reiner–Philippoff fluid parameter (shear thinning) and fluid moves easily near the surface and an augmentation in the skin friction coefficient takes place. Figure 16 provides the explanation regarding the impact of Reiner–Philippoff fluid parameter in three different cases dilatant $\lambda < 1$, Newtonian $\lambda = 1$, and pseudoplastic $\lambda > 1$ versus Bingham number on the skin friction coefficient. It is quite understood that if viscosity of fluid decreases, its surrounding temperature drops gradually. At this stage, the drag coefficient will increase with increase in certain degree of viscosity but opposite behaviour is observed where viscosity increases gradually. In the case of shear thinning ($\lambda < 1$), the viscosity of fluid decreases (shear thinning) which guides to an abatement in the Bingham number (shear thinning) and surface drag

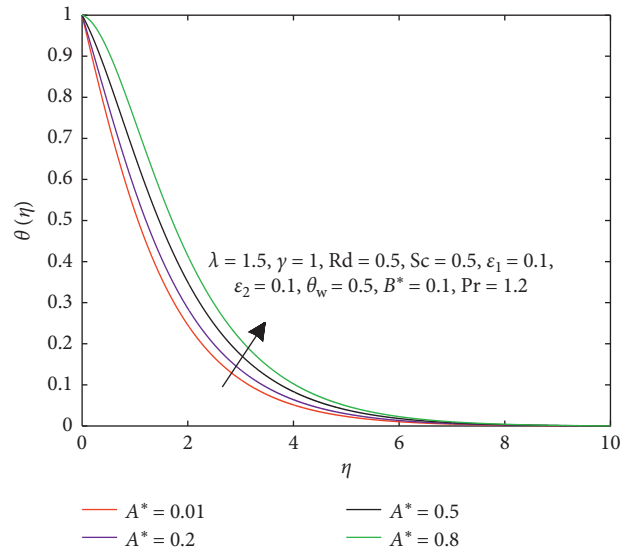

Figure 7: Influence of A^* on θ.

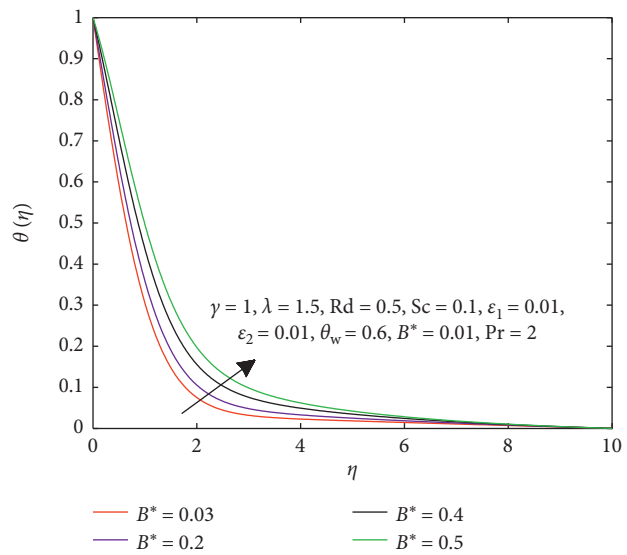

Figure 8: Influence of B^* on θ.

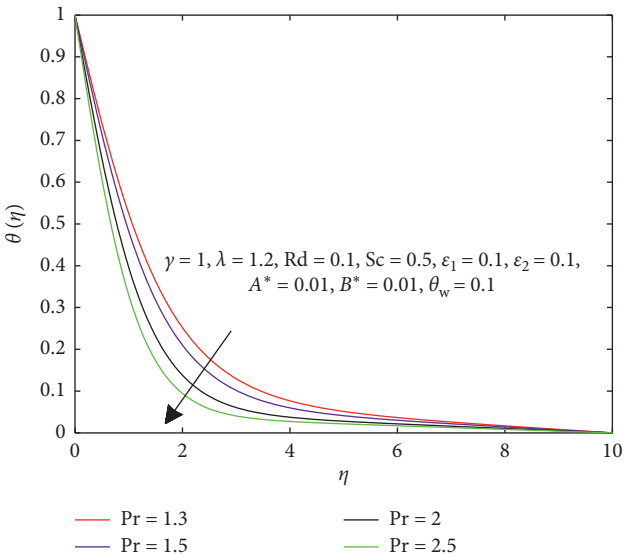

Figure 9: Influence of Pr on θ.

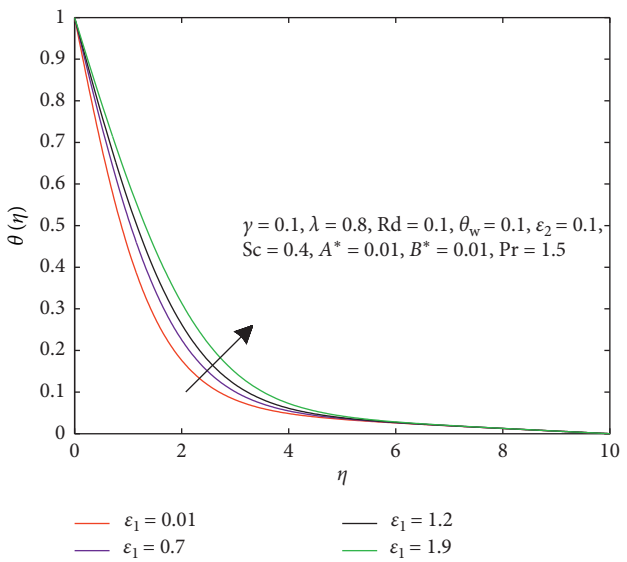

Figure 10: Influence of ϵ_1 on θ.

coefficient but opposite behaviour is observed in the case of $\lambda > 1$ (shear thickening). Figure 17 specifically explains the impact of Prandtl number versus radiation parameter on the heat transfer rate. It is observed that a positive variation in Prandtl number and radiation parameter guides to an improvement in the Nusselt number. Both thermal radiation and Prandtl number are prominent factors of nonlinear thermal radiation which is used where high temperature difference is required. In the presence of nonlinear thermal radiation, heat transfer rate increases. Figure 18 is sketched to interrogate the impact of Prandtl number and temperature ratio parameter on the Nusselt number. Both Prandtl number and temperature ratio parameter are important constituents of nonlinear thermal radiation. The temperature of the fluid increases in the presence of temperature ratio parameter and Prandtl number. As a result, heat transfer rate escalates. Figures 19 and 20 are portrayed to interrogate the impact of space- and temperature-dependent heat source/sink parameter versus Prandtl number on the Nusselt number. It is canvassed that more heat is generated inside the fluid in the case of $A^* > 0$ and $B^* > = 0$. Thermal diffusivity booms because of heat generated inside the fluid by heat source/sink parameter. As a result, Prandtl number decreases which is ratio of momentum diffusivity to thermal diffusivity which leads to a reduction in the heat transfer rate. Figure 21 is designed to discuss the impact of Reiner–Philippoff parameter, i.e., $\lambda < 1$, $\lambda = 1$, and $\lambda > 1$ versus Bingham number on the Nusselt number. In the case of shear thinning fluid ($\lambda < 1$), the viscosity of fluid decreases which eventually guides to an increment in temperature and heat transfer rate booms as well but situation is opposite in the thickening fluid $\lambda = 1$ where an augmentation in viscosity drives to an abatement in temperature and heat transfer rate as well. Figure 22 is portrayed to investigate the impact of Schmidt

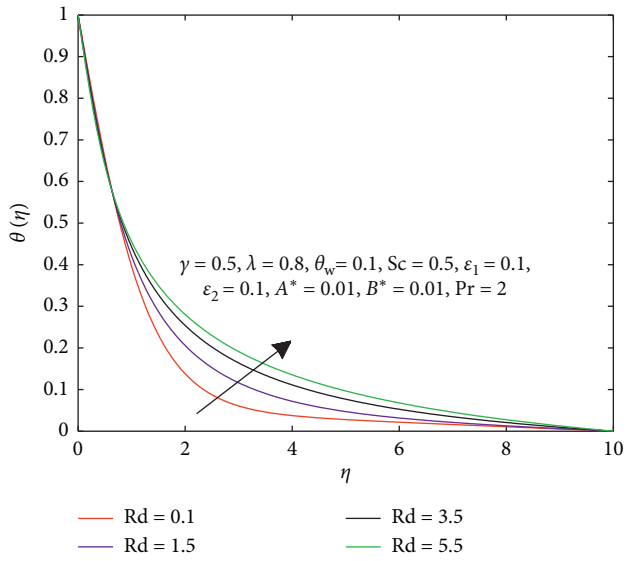

Figure 11: Influence of Rd on θ.

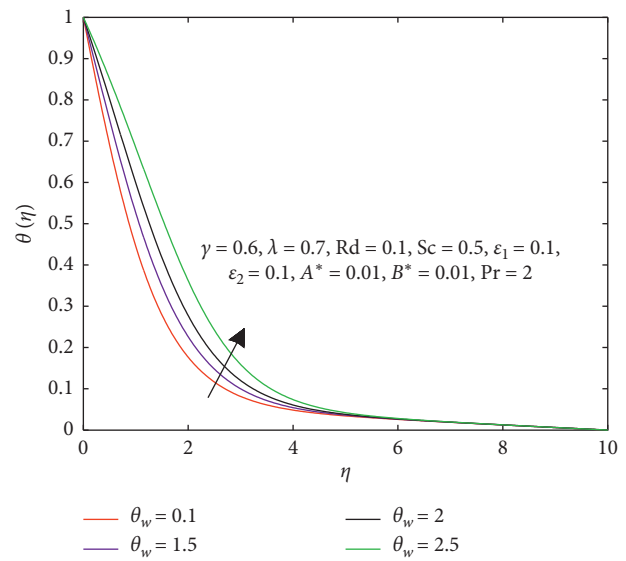

Figure 12: Influence of θ_w on θ.

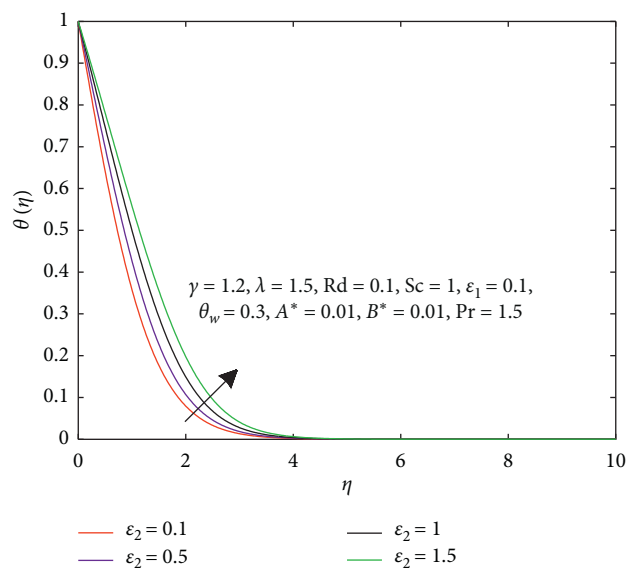

Figure 13: Influence of ϵ_2 on ϕ.

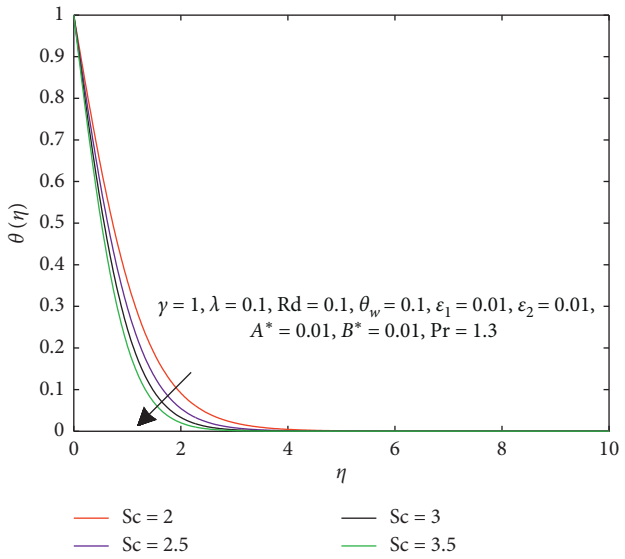

Figure 14: Influence of Sc on ϕ.

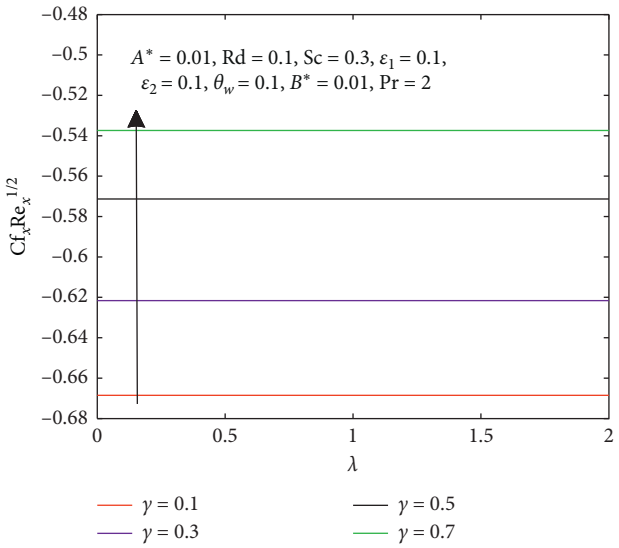

Figure 15: Impact of γ on $Cf_x \mathrm{Re}_x^{1/2}$.

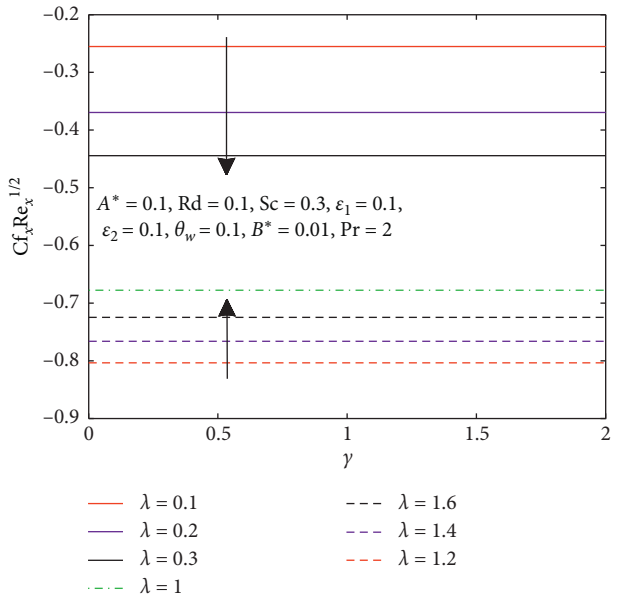

Figure 16: λ versus γ on $Cf_x \mathrm{Re}_x^{-1/2}$.

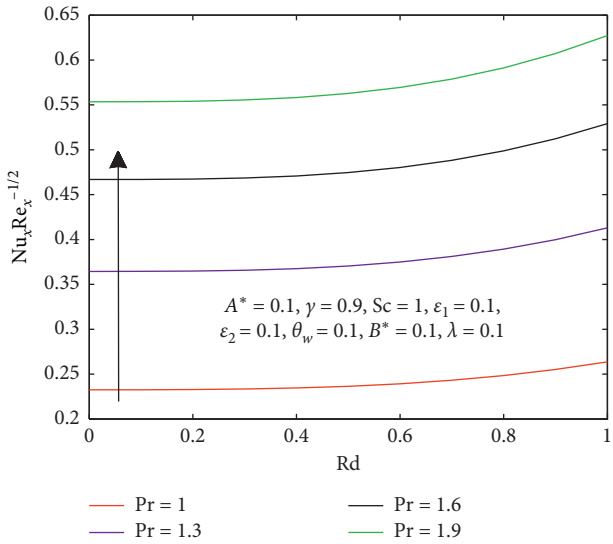

Figure 17: Pr versus Rd on $\mathrm{Nu}_x\mathrm{Re}_x^{-1/2}$.

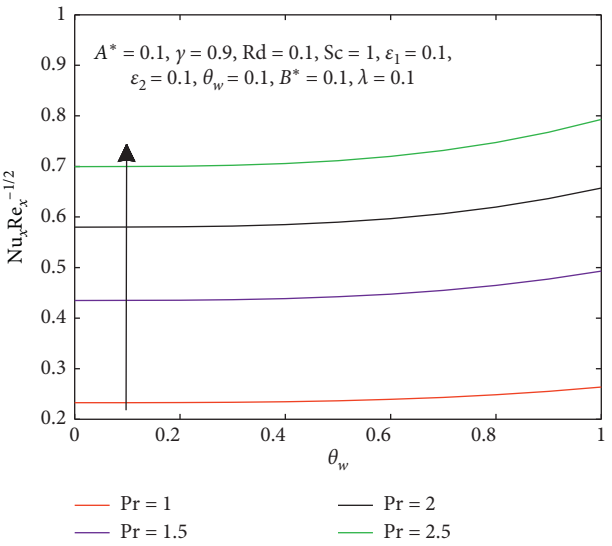

Figure 18: Pr versus θ_w on $\mathrm{Nu}_x\mathrm{Re}_x^{-1/2}$.

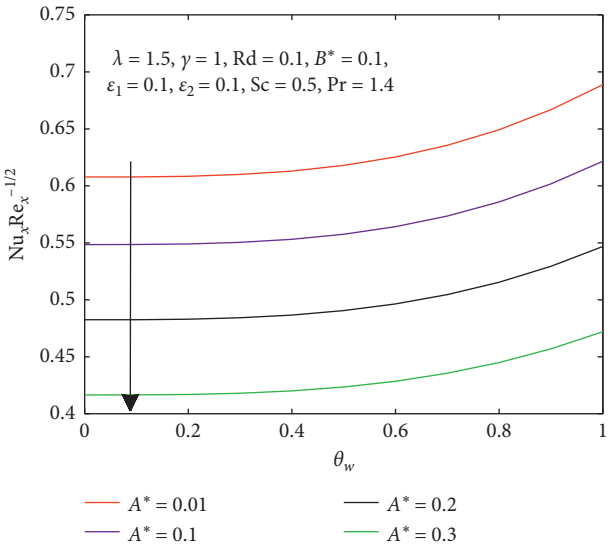

Figure 19: A^* versus θ_w on $\mathrm{Nu}_x\mathrm{Re}_x^{-1/2}$.

number versus variable molecular diffusivity on the Sherwood number. It is observed that the gradual enhancement in Sc tends to weak molecular diffusivity and boundary layer thickness. As a result of this, an augmentation in Sc drives to an improvement in the Sherwood number. Figure 23 is sketched to scrutinize the conduct of variable molecular diffusivity ϵ_2 versus Schmidt number Sc on Sherwood number. It is observed that species diffusivity is directly proportional to concentration. It is perceived that a positive variation in species diffusivity guides to an augmentation in concentration. As a result, Sherwood number enhances.

5. Final Remarks

The research examines the impact of nonlinear thermal radiation, heat source/sink, variable thermal conductivity, and variable molecular diffusivity on Reiner–Philippoff fluid past a stretching sheet. The concluding remarks of the present research are enumerated underneath.

(i) A mitigation in the shear stress field occurs on account of an escalation in the Bingham number γ but a transverse behaviour is monitored in the case of fluid parameter λ.

(ii) Surface drag coefficient abates in the case of dilatant fluid but improves in the case of pseudoplastic fluid.

(iii) An uplift in the thermal conductivity parameter ϵ_1 produces a random movement among the molecules owing to an improvement in the temperature field.

(iv) Temperature ratio parameter θ_w, radiation parameter Rd, and Prandtl number Pr are three

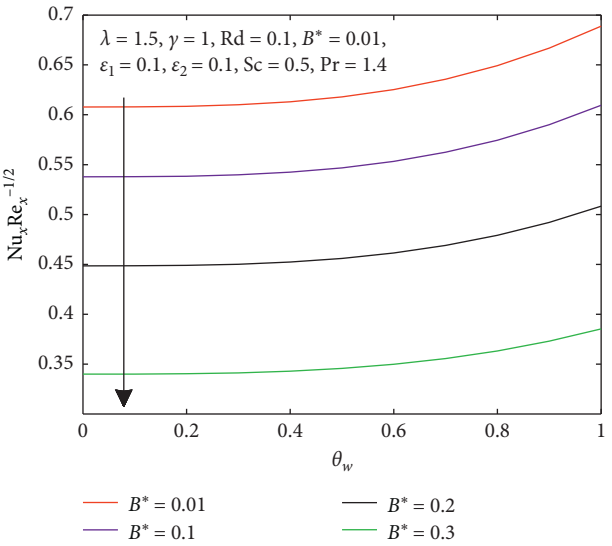

Figure 20: B^* versus θ_w on $\mathrm{Nu}_x\mathrm{Re}_x^{-1/2}$.

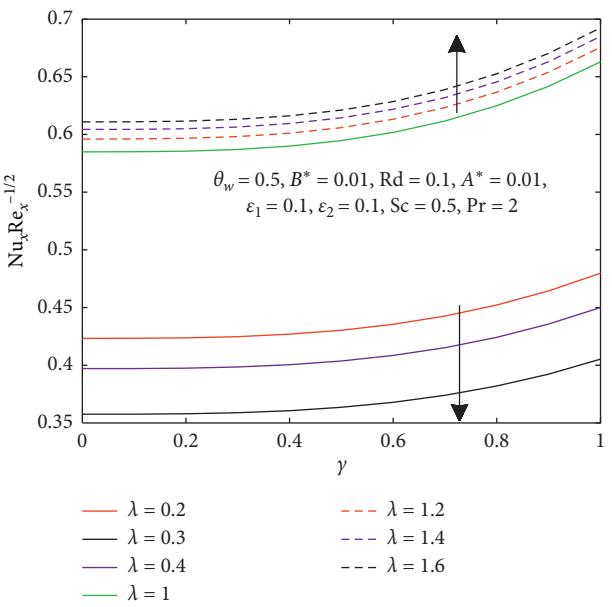

Figure 21: λ versus γ on $\mathrm{Nu}_x\mathrm{Re}_x^{-1/2}$.

prominent factors of nonlinear thermal radiation responsible for an improvement in the temperature field and local Nusselt number.

(v) Heat transfer rate augments in the case of shear thinning fluid but depreciates in the case of shear thickening fluid.

(vi) The upshots revealed that a positive variation in the heat generation/absorption parameters A^* and B^* generates more heat which produces an enlargement in the temperature field.

(vii) A positive variation in the species diffusivity parameter ϵ_2 causes an increment in the mass fraction field.

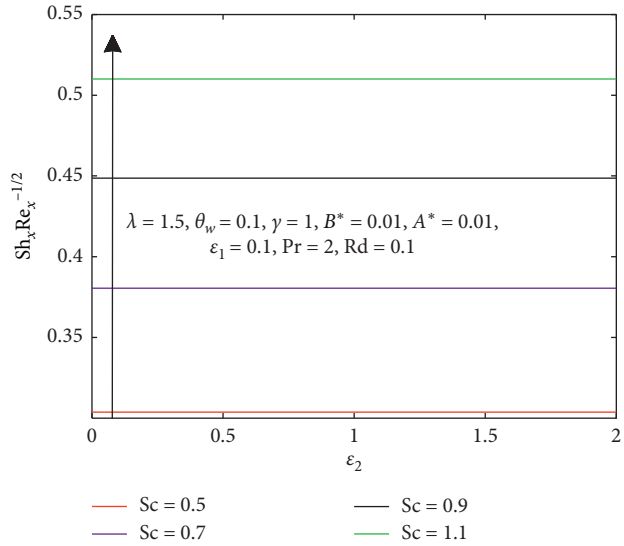

Figure 22: Impact of Sc and ϵ_2 on $\mathrm{Sh}_x\mathrm{Re}_x^{-1/2}$.

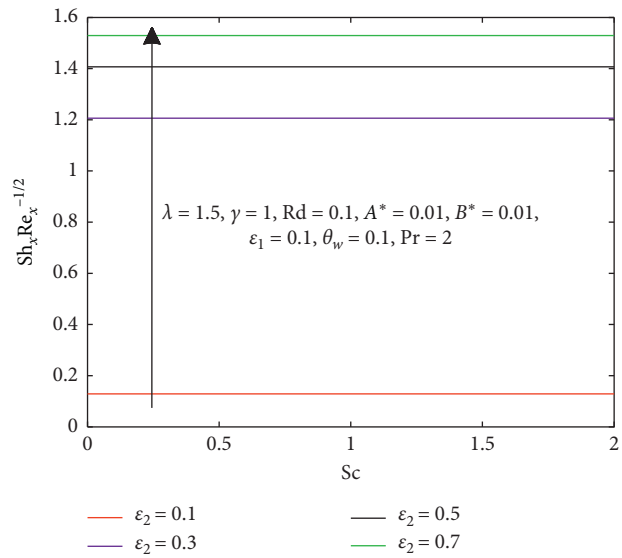

Figure 23: ϵ_2 versus θ_w on $\mathrm{Nu}_x\mathrm{Re}_x^{-1/2}$.

(viii) Augmentation in Schmidt number Sc and variable molecular diffusivity ϵ_2 decreases the local Sherwood number.

Nomenclature

ϵ_2: Variable molecular diffusivity parameter
C: Concentration of fluid
C_0: Wall concentration
C_∞: Ambient concentration
γ: Fluid parameter
j_w: Mass flux
A^*: Heat generation/absorption
Sc: Schmidt number

Nu_x: Nusselt number
Pr: Prandtl number
θ_w: Temperature ratio parameter
τ: Shear stress
μ_0: Shear viscosity
σ^*: Stefan–Boltzmann constant
$(\rho c)_p$: Heat capacity of nanoparticles
ϵ_1: Variable thermal conductivity parameter
D_{B_∞}: Ambient Brownian diffusion coefficient
T_∞: Ambient temperature
$U(x)$: Stretching velocity
λ: Fluid parameter
κ_∞: Ambient fluid thermal conductivity
B^*: Heat generation/absorption
q_w: Surface heat flux
Sh_x: Sherwood number
Rd: Radiation parameter
q_r: Radiative heat flux
τ_s: Reference shear stress
μ_∞: Limiting viscosity
κ^*: Absorption coefficient.

Data Availability

The data supporting the findings of this study are available within the article.

Conflicts of Interest

The authors declare that there are no conflicts of interest regarding the publication of this paper.

References

[1] J. N. Kapur and R. C. Gupta, "Two dimensional flow of Reiner-Philippoff fluids in the inlet length of a straight channel," *Applied Scientific Research, Section A*, vol. 14, pp. 13–24, 1965.

[2] S. Ghoshal, "Dispersion of solutes in non-Newtonian flows through a circular tube," *Chemical Engineering Science*, vol. 26, no. 2, pp. 185–188, 1971.

[3] T. Y. Na, "Boundary layer flow of Reiner-Philippoff fluids," *International Journal of Non-Linear Mechanics*, vol. 29, no. 6, pp. 871–877, 1994.

[4] K. S. Yam, S. D. Harris, D. B. Ingham, and I. Pop, "Boundary-layer flow of Reiner-Philippoff fluids past a stretching wedge," *International Journal of Non-Linear Mechanics*, vol. 44, no. 10, pp. 1056–1062, 2009.

[5] A. Ahmad, "Flow of ReinerPhilippoff based nano-fluid past a stretching sheet," *Journal of Molecular Liquids*, vol. 219, pp. 643–646, 2016.

[6] A. Ahmad, M. Qasim, and S. Ahmed, "Flow of Reiner-Philippoff fluid over a stretching sheet with variable thickness," *Journal of the Brazilian Society of Mechanical Sciences and Engineering*, vol. 39, no. 11, pp. 4469–4473, 2017.

[7] M. G. Reddy, S. Rani, K. G. Kumar, A. H. Seikh, M. Rahimi-Gorji, and E.-S. M. Sherif, "Transverse magnetic flow over a Reiner-Philippoff nanofluid by considering solar radiation," *Modern Physics Letters B*, vol. 33, no. 36, p. 1950449, 2019.

[8] K. G. Kumar, M. V. V. N. L. Sudharani, M. G. Reddy, S. M. Shehzad, and A. J. Chamkha, "Cattaneo-Christov heat diffusion phenomenon in Reiner-Philippoff fluid through a transverse magnetic field," *Physica A: Statistical Mechanics and Its Applications*, p. 123330, 2019.

[9] M. G. Reddy, M. V. V. N. L. Sudharani, K. G. Kumar, A. J. Chamkha, and G. Lorenzini, "Physical aspects of Darcy-Forchheimer flow and dissipative heat transfer of Reiner–Philippof fluid," *Journal of Thermal Analysis and Calorimetry*, vol. 39, pp. 11–25, 2019.

[10] A. Pantokratoras, "Natural convection along a vertical isothermal plate with linear and non-linear Rosseland thermal radiation," *International Journal of Thermal Sciences*, vol. 84, pp. 151–157, 2014.

[11] E. Magyari and A. Pantokratoras, "Note on the effect of thermal radiation in the linearized Rosseland approximation on the heat transfer characteristics of various boundary layer flows," *International Communications in Heat and Mass Transfer*, vol. 38, no. 5, pp. 554–556, 2011.

[12] Y. B. Kho, A. Hussanan, M. K. A. Mohamed, N. M. Sarif, Z. Ismail, and M. Z. Salleh, "Thermal radiation effect on MHD flow and heat transfer analysis of Williamson nanofluid past over a stretching sheet with constant wall temperature," *Journal of Physics: Conference Series*, vol. 890, p. 012034, 2017.

[13] T. Hayat, S. Qayyum, M. Waqas, and A. Alsaedi, "Thermally radiative stagnation point flow of Maxwell nanofluid due to unsteady convectively heated stretched surface," *Journal of Molecular Liquids*, vol. 224, pp. 801–810, 2016.

[14] T. Hayat, M. Waqas, S. A. Shehzad, and A. Alsaedi, "Chemically reactive flow of third grade fluid by an exponentially convected stretching sheet," *Journal of Molecular Liquids*, vol. 223, pp. 853–860, 2016.

[15] M. Waqas, S. A. Shehzad, T. Hayat, M. I. Khan, and A. Alsaedi, "Simulation of magnetohydrodynamics and radiative heat transport in convectively heated stratified flow of Jeffrey nanofluid," *Journal of Physics and Chemistry of Solids*, vol. 133, pp. 45–51, 2019.

[16] M. Waqas, M. I. Khan, T. Hayat, M. M. Gulzar, and A. Alsaedi, "Transportation of radiative energy in viscoelastic nanofluid considering buoyancy forces and convective conditions," *Chaos, Solitons & Fractals*, vol. 130, p. 109415, 2020.

[17] A. López, G. Ibáñez, J. Pantoja, J. Moreira, and O. Lastres, "Entropy generation analysis of MHD nanofluid flow in a porous vertical microchannel with nonlinear thermal radiation, slip flow and convective-radiative boundary conditions," *International Journal of Heat and Mass Transfer*, vol. 107, pp. 982–994, 2017.

[18] M. Farooq, M. I. Khan, M. Waqas, T. Hayat, A. Alsaedi, and M. I. Khan, "MHD stagnation point flow of viscoelastic nanofluid with non-linear radiation effects," *Journal of Molecular Liquids*, vol. 221, pp. 1097–1103, 2016.

[19] M. I. Khan, T. Hayat, M. I. Khan, and A. Alsaedi, "Activation energy impact in nonlinear radiative stagnation point flow of Cross nanofluid," *International Communications in Heat and Mass Transfer*, vol. 91, pp. 216–224, 2018.

[20] T. Hayat, M. I. Khan, S. Qayyum, A. Alsaedi, and M. Imran Khan, "New thermodynamics of entropy generation minimization with nonlinear thermal radiation and nanomaterials," *Physics Letters A*, vol. 91, pp. 216–224, 2018.

[21] S. Qayyum, M. I. Khan, T. Hayat, and A. Alsaedi, "A framework for nonlinear thermal radiation and homogeneous-heterogeneous reactions flow based on silver-water and copper-water nanoparticles: a numerical model for probable error," *Results in Physics*, vol. 7, pp. 1907–1914, 2017.

[22] S. S. Ghadikolaei, K. Hosseinzadeh, D. D. Ganji, and B. Jafari, "Nonlinear thermal radiation effect on magneto Casson

nanofluid flow with Joule heating effect over an inclined porous stretching sheet," *Case Studies in Thermal Engineering*, vol. 12, pp. 176–187, 2018.

[23] M. Waqas, S. Jabeen, T. Hayat, M. I. Khan, and A. Alsaedi, "Modeling and analysis for magnetic dipole impact in nonlinear thermally radiating Carreau nanofluid flow subject to heat generation," *Journal of Magnetism and Magnetic Materials*, vol. 485, pp. 197–204, 2019.

[24] T. Sajid, M. Sagheer, S. Hussain, and M. Bilal, "Darcy-Forchheimer flow of Maxwell nanofluid flow with nonlinear thermal radiation and activation energy," *AIP Advances*, vol. 8, no. 3, p. 035102, 2018.

[25] M. S. Abdel-Wahed, "Nonlinear Rosseland thermal radiation and magnetic field effects on flow and heat transfer over a moving surface with variable thickness in a nanofluid," *Canadian Journal of Physics*, vol. 95, no. 3, pp. 267–273, 2017.

[26] S. Farooq, M. I. Khan, M. Waqas, T. Hayat, and A. Alsaedi, "Transport of hybrid type nanomaterials in peristaltic activity of viscous fluid considering nonlinear radiation, entropy optimization and slip effects," *Computer Methods and Programs in Biomedicine*, vol. 184, p. 105086, 2019.

[27] T. Hayat, M. Waqas, S. A. Shehzad, and A. Alsaedi, "On 2D stratified flow of an Oldroyd-B fluid with chemical reaction: an Application of non-Fourier heat flux theory," *Journal of Molecular Liquids*, vol. 223, pp. 566–571, 2016.

[28] M. W. A. Khan, M. I. Khan, T. Hayat, and A. Alsaedi, "Entropy generation minimization (EGM) of nanofluid flow by a thin moving needle with nonlinear thermal radiation," *Physica B: Condensed Matter*, vol. 534, pp. 113–119, 2018.

[29] S. Reddy, K. Naikoti, and M. M. Rashidi, "MHD flow and heat transfer characteristics of Williamson nanofluid over a stretching sheet with variable thickness and variable thermal conductivity," *Transactions of A. Razmadze Mathematical Institute*, vol. 171, pp. 195–211, 2017.

[30] T. Hayat, M. Zubair, M. Waqas, A. Alsaedi, and M. Ayub, "On doubly stratified chemically reactive flow of Powell-Eyring liquid subject to non-Fourier heat flux theory," *Results in Physics*, vol. 7, pp. 99–106, 2017.

[31] R. V. M. S. S. K. Kumar and S. V. K. Varma, "MHD boundary layer flow of nanofluid through a porous medium over a stretching sheet with variable wall thickness: using Cattaneo-Christov heat flux model," *Journal of Theoretical and Applied Mechanics*, vol. 48, pp. 72–92, 2018.

[32] T. E. Akinbobola and S. S. Okoya, "The flow of second grade fluid over a stretching sheet with variable thermal conductivity and viscosity in the presence of heat source/sink," *Journal of the Nigerian Mathematical Society*, vol. 34, no. 3, pp. 331–342, 2015.

[33] M. Waqas, T. Hayat, M. Farooq, S. A. Shehzad, and A. Alsaedi, "Cattaneo-Christov heat flux model for flow of variable thermal conductivity generalized Burgers fluid," *Journal of Molecular Liquids*, vol. 220, pp. 642–648, 2016.

[34] M. Ramzan, M. Bilal, S. Kanwal, and J. D. Chung, "Effects of variable thermal conductivity and nonlinear thermal radiation past an Eyring-Powell nanofluid flow with chemical reaction," *Communications in Theoretical Physics*, vol. 67, no. 9, 2017.

[35] R. Cortell, "Heat transfer in a fluid through a porous medium over a permeable stretching surface with thermal radiation and variable thermal conductivity," *The Canadian Journal of Chemical Engineering*, vol. 90, no. 5, pp. 1347–1355, 2012.

[36] M. Irfan, M. Khan, and W. A. Khan, "Numerical analysis of unsteady 3D flow of Carreau nanofluid with variable thermal conductivity and heat source/sink," *Results in Physics*, vol. 7, pp. 3315–3324, 2017.

[37] T. Hayat, H. Khalid, M. Waqas, and A. Alsaedi, "Numerical simulation for radiative flow of nanoliquid by rotating disk with carbon nanotubes and partial slip," *Computer Methods in Applied Mechanics and Engineering*, vol. 7, pp. 3315–3324, 2017.

[38] M. Waqas, "A mathematical and computational framework for heat transfer analysis of ferromagnetic non-Newtonian liquid subjected to heterogeneous and homogeneous reactions," *Journal of Magnetism and Magnetic Materials*, vol. 493, p. 165646, 2020.

[39] A. M. Salem and M. Abd El-Aziz, "Effect of Hall currents and chemical reaction on hydromagnetic flow of a stretching vertical surface with internal heat generation/absorption," *Applied Mathematical Modelling*, vol. 32, no. 7, pp. 1236–1254, 2008.

[40] T. Hayat, S. Naz, M. Waqas, and A. Alsaedi, "Effectiveness of Darcy-Forchheimer and nonlinear mixed convection aspects in stratified Maxwell nanomaterial flow induced by convectively heated surface," *Applied Mathematics and Mechanics*, vol. 39, no. 10, pp. 1373–1384, 2018.

[41] S. P. A. Devi, M. Agneeshwari, and J. W. S. Raj, "Radiation effects on MHD boundary layer flow and heat transfer over a nonlinear stretching surface with variable wall temperature in the presence of non-uniform heat source/sink," *International Journal of Applied Mechanics and Engineering*, vol. 23, no. 2, pp. 289–305, 2018.

[42] M. Muthtamilselvan and E. Ramya, "Heat transfer in a liquid film over an unsteady porous stretching sheet with different boundary conditions," *Australian Journal of Mechanical Engineering*, 2016.

[43] T. Hayat, M. I. Khan, M. Waqas, and A. Alsaedi, "On the performance of heat absorption/generation and thermal stratification in mixed convective flow of an Oldroyd-B fluid," *Nuclear Engineering and Technology*, vol. 49, no. 8, pp. 1645–1653, 2017.

[44] A. K. A. Hakeem, B. Ganga, S. M. Y. Ansari, N. V. Ganesh, and M. M. Rahman, "Nonlinear studies on the effect of non-uniform heat generation/absorption on hydromagnetic flow of nanofluid over a vertical plate," *Nonlinear Analysis: Modelling and Control*, vol. 22, pp. 1–16, 2017.

[45] M. A. El-Aziz and A. M. Salem, "MHD-mixed convection and mass transfer from a vertical stretching sheet with diffusion of chemically reactive species and space- or temperature-dependent heat source," *Canadian Journal of Physics*, vol. 85, no. 4, pp. 359–373, 2007.

[46] S. K. Adegbie, O. K. Kọrikọ, and I. L. Animasaun, "Melting heat transfer effects on stagnation point flow of micropolar fluid with variable dynamic viscosity and thermal conductivity at constant vortex viscosity," *Journal of the Nigerian Mathematical Society*, vol. 35, no. 1, pp. 34–47, 2016.

[47] T. Hayat, M. Waqas, M. I. Khan, and A. Alsaedi, "Analysis of thixotropic nanomaterial in a doubly stratified medium considering magnetic field effects," *International Journal of Heat and Mass Transfer*, vol. 102, pp. 1123–1129, 2016.

[48] K. Avinash, N. Sandeep, and O. D. Makinde, "Non-uniform heat source/sink effect on liquid film flow of Jeffrey nanofluid over a stretching sheet," *Diffusion Foundations*, vol. 11, pp. 72–83, 2017.

[49] D. H. Doh, M. Muthtamilselvan, and D. Prakash, "Transient heat and mass transfer of micropolar fluid between porous vertical channel with boundary conditions of third kind,"

International Journal of Nonlinear Sciences and Numerical Simulation, vol. 17, pp. 231–242, 2016.

[50] D. H. Doh, M. Muthtamilselvan, B. Swathene, and E. Ramya, "Homogeneous and heterogeneous reactions in a nanofluid flow due to a rotating disk of variable thickness using HAM," *Mathematics and Computers in Simulation*, vol. 17, pp. 231–242, 2019.

[51] T. Y. Na, *Computational Methods in Engineering Boundary Value Problems*, Academic Press, Cambridge, MA, USA, 1979.